PHYSOR 2012 Advances in Reactor Physics Linking Research, Industry, and Education
Knoxville, Tennessee, USA, April 15-20, 2012, on CD-ROM, American Nuclear Society, LaGrange Park, IL (2012)

EXPERIMENTAL VALIDATION OF CASMO-4E AND CASMO-5M FOR RADIAL FISSION RATE DISTRIBUTIONS IN A WESTINGHOUSE SVEA-96 OPTIMA2 BWR FUEL ASSEMBLY

Peter Grimm and Gregory Perret
Paul Scherrer Institute
CH-5232 Villigen PSI
Switzerland
Peter.Grimm@psi.ch; Gregory.Perret@psi.ch

ABSTRACT

Measured and calculated radial total fission rate distributions are compared for the three axial sections of a Westinghouse SVEA-96 Optima2 BWR fuel assembly, comprising 96, 92 and 84 fuel rods, respectively. The measurements were performed on a full-size fuel assembly in the PROTEUS zero-power experimental facility. The measured fission rates are compared to the results of the CASMO-4E and CASMO-5M fuel assembly codes. Detailed measured geometrical data were used in the models, and effects of the surrounding zones of the reactor were taken into account by correction factors derived from MCNPX calculations. The results of the calculations agree well with those of the experiments, with root-mean-square deviations between 1.2% and 1.5% and maximum deviations of 3–4%. The quality of the predictions by CASMO-4E and CASMO-5M is comparable.

Key Words: Boiling water reactors, part-length fuel rods, pin power distributions, integral experiments, assembly codes

1. INTRODUCTION

With the aim of increasing discharge burnups and enhancing operational flexibility, highly heterogeneous fuel assembly designs for boiling water reactors (BWR) have been developed in recent years. In addition to the material heterogeneities caused by the presence of fuel rods with different enrichments and a relatively large number of burnable absorber (BA) fuel rods, these assemblies also feature geometrically complex internal bypass regions designed to flatten the thermal neutron flux distribution across the assemblies. This complexity calls for experimental validation of the calculational codes used for core design and monitoring, but experiments performed in the past were typically representative of the less challenging assembly designs used at that time.

The LWR-PROTEUS experimental program, conducted in a collaboration between the Swiss nuclear utilities (swiss*nuclear*) and the Paul Scherrer Institute (PSI), aimed at improving the validation base for modern LWR fuel designs. Full-size power reactor fuel assemblies were investigated in a zero-power experimental reactor before being loaded in the power plant. In particular, Westinghouse SVEA-96+/L and SVEA-96 Optima2 assemblies were measured in Phases I and III of the program, respectively.

In this paper, the radial fission rate distributions calculated using the CASMO-4E and CASMO-5M fuel assembly codes are compared to those measured in the different axial sections of a SVEA-96 Optima2 assembly in Phase III of the program. It complements the comparison of MCNPX results against the same experimental data reported previously [1–3].

2. LWR-PROTEUS PHASE III CONFIGURATIONS AND MEASUREMENTS

The LWR-PROTEUS experimental program was performed in the PROTEUS zero-power critical facility at PSI. PROTEUS is a driven reactor, in which a subcritical central test zone is driven critical by the surrounding regions. For the LWR-PROTEUS experiments the test zone, constituted by actual power reactor fuel, was contained in a 45×45 cm^2 aluminum tank. This region was surrounded, from inside to outside, by a natural uranium metal buffer, two driver regions moderated with heavy water and graphite, respectively, and a graphite reflector. The two driver regions were fueled with 5%-enriched UO_2. All the control and shutdown rods as well as the reactor instrumentation are located in the graphite region, thus avoiding any spectral perturbations by these in the test zone. Since the commercial reactor fuel used for the experiments has an active length of almost 4 m and the driver is only approximately 1 m high, the test tank can be moved axially, so that different axial zones of the fuel assemblies can be investigated.

The test zone for the LWR-PROTEUS Phase III experiments was constituted of an array of 3×3 Westinghouse SVEA-96 Optima2 BWR fuel assemblies. The central assembly, in which the measurements were performed, and the eight surrounding assemblies are of two different nuclear designs. The two designs are geometrically identical, but they differ in the enrichments of the fuel rods as well as in the number and Gd concentration of burnable poison fuel rods. The assemblies consist of four subbundles of 24 fuel rods each, which are arranged around a water cross (diamond-shaped central canal and four wings) as shown in Figure 1. In the Optima2 design only 84 of the 96 fuel rods span the full active length. The four fuel rods at the outer corners of the assembly extend from the bottom to approximately one third of the height and the eight rods surrounding the central water canal to two thirds. The assembly thus consists of three axial sections featuring 96, 92 and 84 fuel rods, respectively.

For all the experiments considered here, the test zone was moderated by a mixture of light water and heavy water with a proportion of 33.7 mol-% D_2O, simulating the number density of hydrogen in non-boiling light water at the operating temperature of a BWR. Measurements were performed at two different axial locations of the BWR assemblies in Cores III-1 and III-2. In Core III-1, the test tank was positioned such that the upper end of the enriched fuel in the one-third part-length fuel rods coincided with the mid-plane of the PROTEUS driver zones. For Core III-2, the test tank was moved down in order to align the tips of the two-third part-length fuel rods with the driver mid-plane.

Total fission rate distributions were measured by γ-ray spectrometry of selected fuel rods. After irradiation in PROTEUS for one hour, up to 10 fuel rods were transferred to an automated γ-ray scanning machine and spectra were acquired for several hours. Fission rates were deduced from the intensities of γ-ray lines of the fission products ^{135}Xe, ^{143}Ce and ^{133}I.

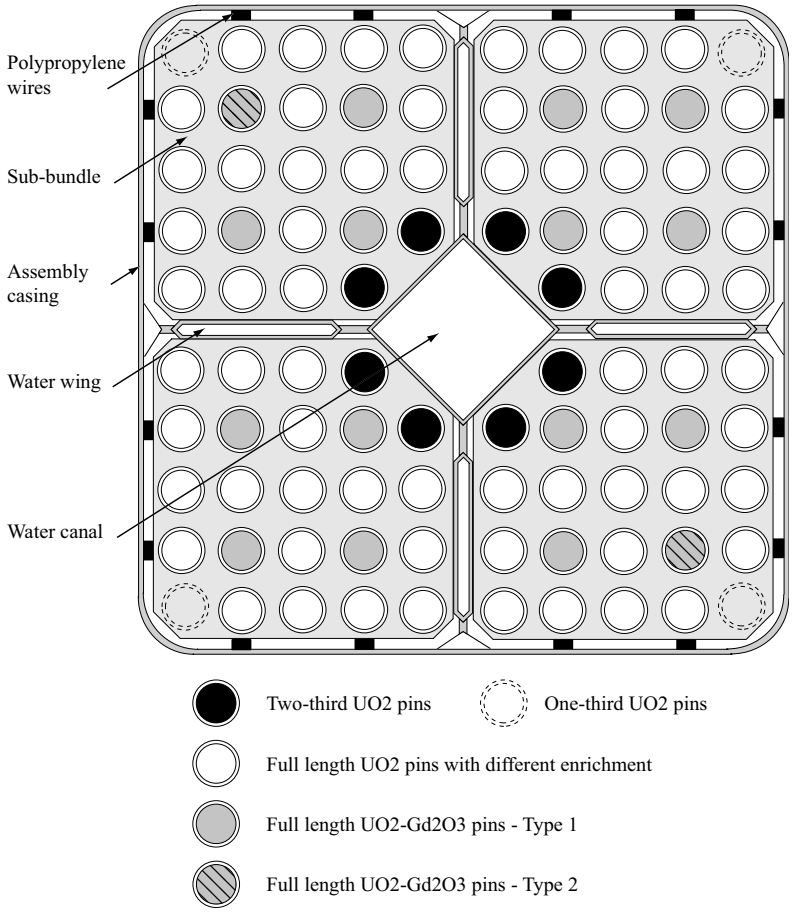

Figure 1. Radial cross-section of a SVEA-96 Optima2 fuel assembly

Special emphasis was given in the LWR-PROTEUS Phase III experiments to measurements of axial reaction rate distributions in fuel rods adjacent to the part-length fuel rods near the upper ends of the latter. The present paper, however, deals with the validation of two-dimensional assembly calculations. Therefore, the calculated fission rate distributions are compared to two-dimensional radial maps measured at a sufficient distance from the tips of the part-length fuel rods where these distributions are not influenced by neighboring axial zones. The calculated radial fission rate maps are compared to measurements performed below the tips of the 1/3 part-length fuel rods (Core III-1) for the 96-rod section and some 20 cm on either side of the tips of the 2/3-length rods (Core III-2) for the 92- and 84-rod sections.

As the fission rate distributions in SVEA-96 assemblies are very sensitive to geometrical details (see e.g. Ref. [1]), it is important to model the as-built geometry of the test zone as accurately as feasible. The widths of the gaps between the fuel assemblies constituting the test zone were measured over the full height of the core at two locations per gap. In addition, the subbundles of the central test assembly were pressed towards the central water cross by fixing polypropylene wires to the edges of the subbundles facing the outer channel. The measured displacement of the subbundles from the nominal positions (centered in their respective subchannels) is

0.50±0.05 mm. This position of the subbundles is representative of the conditions in an operating BWR, the subbundles being pressed towards the center of the assembly by hydraulic forces. In the eight outer fuel assemblies of the test zone the subbundles were pulled towards the center only at the top. It was assumed that the subbundles were centered in the subchannels at the bottom and that the displacement varies linearly as a function of height. Thus, it was inferred that the subbundles were moved inward from the nominal positions by 0.17 mm at the elevation where the measurements in Core III-1 were performed and by 0.32 mm for Core III-2 [1,3].

3. CALCULATIONS

3.1. Codes and Cross Section Libraries Used

The fission rate distributions in the test assembly were calculated using the CASMO-4E and CASMO-5M codes. CASMO-4E [4] (where the letter "E" stands for "extended") is an advanced version of the well-known CASMO-4 fuel assembly transport and depletion code. A key feature of CASMO-4 is the characteristics method used for the two-dimensional transport calculations, which allows an explicit representation of the geometry of the assembly without homogenization of pin-cells. CASMO-4E version 2.10.15 was used for the work reported here in conjunction with the E6LIB update D cross-section library, based on ENDF/B-VI nuclear data.

CASMO-5M [5] (the letter "M" stands for "multi-assembly") is the successor to CASMO-4E. The basic calculational methods of CASMO-5M are similar to those of CASMO-4E. A new capability of CASMO-5M of interest for the application described here is that the central water canal of the SVEA-96 assembly can be modeled in its real orientation, whereas in CASMO-4E it is represented parallel to the outer walls of the assembly channel, i.e. rotated by 45°. Other differences between the methods of CASMO-5 and CASMO-4, viz. improvements in the calculation of the Dancoff factors, in the polar angle integration and for the depletion of Gd burnable poison, are already implemented in CASMO-4E. Important differences between CASMO-5M and CASMO-4E exist in the energy group structures used at the various stages of the calculations. The cross-section library of CASMO-5M contains data in 586 groups as opposed to 70 groups for CASMO-4E. In particular, the CASMO-5M structure is very fine in the resolved resonance range below 10 eV (375 groups between 0.625 eV and 10 eV), so that the resonance self-shielding and possible overlaps of resonances of different nuclides are treated directly in the micro-group (pin-cell) calculation without the need for a separate resonance self-shielding calculation in this energy range. The default group structure for the two-dimensional characteristics calculations (for UO_2 fuel) has also been refined from 8 groups in CASMO-4E to 19 groups in CASMO-5M. In contrast to CASMO-4E, CASMO-5M does not use a macro-group calculation (intermediate step of group collapsing between the pin-cell and two-dimensional calculations), the characteristics calculations being carried out in a larger number of groups. It is also important to mention that the cross-section library for CASMO-5M is based on the recent ENDF/B-VII.0 evaluation and the library is not adjusted. CASMO-5M version 1.06.00 and the E7R0LIB, update E cross-section library were used for the calculations described here.

3.2. Models and Options Used

All the results presented in this paper were obtained from calculations for a model of a single assembly with reflective boundary conditions. The calculations were carried out for a full assembly without diagonal symmetry due to the asymmetries of the measured inter-assembly water gaps. Correction factors were applied to the results of these calculations to account for whole-reactor effects which cannot be simulated using this model (see Section 3.4 below).

Measured geometrical data were used in all calculations. This means that the subbundles were displaced 0.50 mm from their nominal positions towards the central water cross. The fact that the subbundles in the outer fuel assemblies of the test zone were moved a smaller distance away from their nominal positions was taken into account by the correction factors. The widths of the inter-assembly water gaps at the elevations where the measurements were performed were deduced from the measured axial profiles of these gaps. The south and east gaps are wider and the north and west gaps narrower than the nominal value, with maximum deviations of slightly more than 1 mm. Half of these gaps were included in the CASMO models on each side of the assembly.

The calculations were performed in a manner representative of routine production calculations, using largely the built-in default options and standard modeling. Thermal expansion and Xe-equilibrium estimate were deactivated. The two-dimensional transport calculations were carried out using the default energy-group structures of the respective code versions (for UO_2 fuel), viz. 8 groups in CASMO-4E and 19 groups in CASMO-5M. In CASMO-5M the central water canal was modeled in its real orientation. The fission rate distributions were determined using the fundamental mode spectrum, i.e. applying the critical axial buckling searched for automatically by the code.

3.3. Effects of the Measured Geometry and of the Surrounding Fuel Assemblies

The effects of the differences between nominal and measured geometrical data as well as of the surrounding assemblies in the Phase III test zone on the fission rate distributions were investigated for the 96-rod section using CASMO-4E.

The position of the subbundles and the widths of the inter-assembly water gaps were changed separately from their nominal to the measured values in calculations for a single reflected assembly. The displacement of the subbundles by 0.5 mm towards the central water cross reduces the total fission rates of the fuel rods adjacent to the central canal by 4% and increases those of the rods at the outer corners of the assembly by almost the same amount.

The change in the inter-assembly gaps affects primarily the peripheral fuel rods. Higher fission rates were found for measured gap widths in the rods along the south and east gaps (which are wider than nominal) and lower ones on the north and west sides (with smaller than nominal widths). The largest differences amount to almost 3%. As a rule of thumb, the fission rates of peripheral fuel rods change by some 2% for a 1 mm difference in the gap width. The effects of both the subbundle position and the water gaps are quantitatively consistent with those found for LWR-PROTEUS Phase I and in MCNPX calculations for the configurations investigated here [1].

The outer assemblies of the test zone differ from the central test element in material compositions (particularly by fewer Gd-poisoned fuel rods and lower enrichments of the peripheral fuel rods) and in the position of the subbundles (cf. Section 2). CASMO-4E calculations for an array of 2×2 assemblies (a so-called colorset) have been performed to study the effects of these differences on the fission rate distribution in the central assembly. The configuration consisted of the central assembly and three of the type of its neighbors, with periodic boundary conditions simulating the impact of the latter on all four sides of the former.

The impact of the differences in the enrichments of the peripheral fuel rods on the fission rate distribution cannot be distinguished from the more important effect of the in-current from the more reactive outer test zone assemblies which increases the fission rates at the periphery of the central assembly. Comparisons of spectral indices have however indicated a slight softening of the neutron spectrum at these locations in the multi-assembly configuration.

The difference in the positions of the subbundles has an effect of similar magnitude as a change in the inter-assembly gaps by the same amount. The total fission rates at the outer corners of the central assembly are 0.6% lower and those in the center 0.5% higher in the configuration of Core III-1 (with subbundles moved towards the water cross 0.50 mm in the central assembly and 0.17 mm in the outer ones) than in a case in which the subbundles of all the assemblies were displaced by 0.50 mm.

3.4. Correction Factors

Reaction rate distributions calculated using a reflected-assembly model cannot be directly compared to measurements on individual rods in the central test assembly which is part of a larger reactor. One effect that impacts these distributions is the global radial flux shape in the PROTEUS reactor, which arises as a consequence of the fact that the k_∞ of the assembly is larger than unity, but the actual reactor is critical. Moreover, heterogeneities and geometrical irregularities of the test zone affect the neutron flux distribution in the test assembly, particularly in the fuel rods at its outer edge, as discussed above.

Correction factors which take the above effects into account were applied to the results of the reflected-assembly calculations. These correction factors were determined as the ratios of MCNPX results from a whole-reactor model [2] and for a reflected assembly. Measured dimensions, particularly for the water gaps between the assemblies and the positions of all subbundles were modeled for these calculations. The reflected-assembly models included the half-widths of the water gaps (consistently with the CASMO models), and reflective boundary conditions were applied at the outer surfaces in the radial direction. Vacuum boundary conditions were used at the bottom and top surfaces and the height was adjusted so as to render the configuration critical. Critical heights for the 96- and 92-rod lattices were found to be 80 cm and 100 cm, respectively. For the 84-rod lattice, an infinitely high assembly was simulated because its k_∞ is slightly less than unity.

MCNPX version 2.5 [6] and a cross-section library based on ENDF/B-VI release 2 were used for these calculations. In the whole-reactor calculations, the fission rates were tallied over axial sections of 18 cm length in regions not perturbed by axial heterogeneities and including the measurement positions. The relatively large value of 18 cm was chosen in order to improve the

statistical precision of the results. In the reflected-assembly models, the reaction rates were averaged over an axial section of ± 10 cm around the axial mid-plane. Typical statistical uncertainties for the correction factors , i.e. the ratios of the pin-wise fission rates in the two configurations, are 0.2%–0.3% (1σ).

The correction factors for all the pins lie within the range 0.98 to 1.02, i.e. very close to unity, showing that the global radial flux curvature and the impact of the surrounding assemblies on the fission rates in the central assembly are small. A systematic trend with peaks at the outer corners and a slight depression in the center of the assembly can be seen for the 84-rod section. This is a consequence of the net radial in-current into this region whose k_∞ is somewhat less than unity. The corrections for the 92-rod section have a less pronounced, but qualitatively similar variation, whereas for the 96-rod section no significant trend (compared to the statistical fluctuations) can be detected.

4. RESULTS AND COMPARISON WITH EXPERIMENTS

The calculated (C) results are compared to the experimental (E) values in terms of C/E ratios for each measured fuel rod. For this comparison, the calculated fission rates were first multiplied by the correction factors from MCNPX (see Section 3.4). Then, both the calculated and experimental distributions were normalized to an average of 1.0 in all the measured rods. It should be noted that with this normalization the average of all the C/E values is close to, but not exactly equal to unity. In addition to the C/E maps, the root-mean-square (rms) deviations of the C/E values from unity and the largest negative and positive deviations are shown below.

The uncertainties of the measured values and of the correction factors were combined quadratically and amount to typically 0.6%. The major contribution to these uncertainties comes from the experiments. These uncertainties do not include any contribution from the calculations and/or the input data (e.g. the geometry of the assemblies). As the investigation presented in Section 3.3 show, small changes in some geometrical quantities can have effects on the fission rate distributions which are larger than the experimental uncertainties.

4.1. CASMO-4E Results

The C/E ratios for the total fission rates calculated by CASMO-4E in the three axial sections are shown in Figure 2. The root-mean-square deviations amount to 1.2%–1.3% for all the three cases and the largest positive and negative deviations to 3–4%. In all the cases, the rms deviations clearly exceed the uncertainties of the measurements of typically 0.6%; this shows that the observed deviations are primarily due to the calculational results. The maximum and minimum C/E values do not systematically occur in certain types of rod locations.

The most clearly visible and systematic trend is a slight underprediction (1–2% in average) of the fission rates of the rods adjacent to the central canal (except for the 84-rod section in which these rods are not present). All the C/E values for these rods in the 96 and 92-rod sections are less than 1.0. For the rods next to the corners (i.e. J9, I10, B10 etc.), there are more positive than negative deviations in all the cases. This trend is qualitatively similar to that observed for the MCNPX results, especially in the 92 and 84-rod sections with missing corner rods [1,3], but somewhat less pronounced.

a) 96-rod axial section

	10	9	8	7	6	5	4	3	2	1
J	0.986	0.999	1.004	1.003	0.999	0.992	0.990	0.999	1.022	0.976
I	1.017	0.987	1.010		1.003	0.991		0.997	1.000	1.007
H		1.002			0.995	0.990			0.998	0.997
G	1.014		0.996	0.985		0.988	0.989	1.006		1.000
F	0.993	1.005	1.002	0.998				0.983		1.007
E	0.993	1.001	0.993	0.978			0.986	0.986	1.003	
D			1.003	1.004	0.991	0.980	0.999	0.992		1.010
C	0.996	1.010		0.991	0.993	0.992	1.000		1.028	1.018
B	0.989	1.022	1.002		1.002	1.003		1.005	1.040	1.034
A	0.997	1.006	1.003	1.014	1.003	1.001	0.997	1.015	1.001	1.003

RMS = 1.2% Max. = 1.040 Min. = 0.976

b) 92-rod axial section

	10	9	8	7	6	5	4	3	2	1
J		1.021	0.992	0.995	0.995	1.002	0.999	1.015	1.017	
I	1.006	0.981	1.004		1.003	0.994		0.999	0.985	1.002
H	1.008	1.013		0.999		0.986	0.988		1.000	1.007
G	1.005		0.999	1.018	0.971	0.978		0.995		1.007
F	0.995	0.994	0.985	0.972			0.976		1.004	1.012
E	1.006	0.999					0.969		1.015	1.012
D	0.989		0.997	1.004	0.981	0.971	1.015	0.998		1.023
C	0.993	1.014		0.979	0.986	0.994	1.007		1.020	1.022
B	0.993	0.979	1.002		0.992	0.996		1.006	0.978	1.013
A		1.022	1.012	1.001	0.998	0.991	1.003	1.005	1.004	

RMS = 1.3% Max. = 1.023 Min. = 0.969

c) 84-rod axial section

	10	9	8	7	6	5	4	3	2	1
J		1.002	0.982	1.002	0.984	0.991	0.988	1.000	1.011	
I	0.998	0.958	1.004		1.002	0.998		1.008	0.971	0.991
H	1.001	1.027		1.002		0.998	1.000		1.017	0.995
G	1.005		1.000	0.979				1.000		1.002
F	0.985	0.996	0.995						0.999	0.993
E	0.992	0.999							1.008	1.004
D	0.987		0.998	0.996			0.990	0.994		1.004
C	0.994	1.005		0.993	0.999	1.000	1.008		1.022	1.010
B	0.990	0.980	1.007		0.988	1.004		0.989	0.973	1.013
A		1.026	0.993	1.017	0.996	0.996	1.012	0.994	1.020	

RMS = 1.2% Max. = 1.027 Min. = 0.958

Figure 2. C/E ratios for the CASMO-4E results (Gd-poisoned rods are shown with a shaded background)

The deviations of the calculated fission rates for the Gd-poisoned rods from the experimental values are not systematic. Only in the 84-rod section the fission rates of all these rods are underestimated by an average of 2%. A comparable underprediction can also be observed for the BA rods near the outer corners of the assembly in the 92-rod section, but the fission rates of those rods near the central canal are overestimated (however not exceeding 2σ of the combined uncertainties). For the 96-rod section, C/E ratios for the Gd rods smaller and greater than unity more or less balance each other. These findings are in contrast to those for a SVEA-96+/L assembly with full-density light-water moderation in LWR-PROTEUS Phase I [7], for which a systematic underestimate by approximately 2% in average was observed with all the calculational methods applied. The deviations for the Gd-poisoned rods appear to be correlated to the neutron spectrum, becoming more negative for a softer spectrum (the water-to-fuel volume ratio increases from the 96 to the 92 and particularly to the 84-rod section, and in Phase I the moderator was full-density H_2O as opposed to the H_2O/D_2O mixture used in Phase III).

A certain concentration of high C/E ratios can generally be seen near the southeast corner of the assembly. This trend is particularly pronounced for the 96-rod lattice. An analogous trend was also found for the 96-rod lattice in the MCNPX results [2]. This gives rise to the suspicion that the geometry of the experimental configuration may not have been modeled accurately in all details.

4.2. CASMO-5M Results

Before discussing the comparison of CASMO-5M results to the experiments, it is interesting to briefly describe the differences of the fission rate distributions calculated by CASMO-5M and CASMO-4E.

The differences in the total fission rates are practically all within $\pm 1.5\%$. The fission rates of the rods surrounding the central water canal from CASMO-5M are approximately 1% higher than the CASMO-4E results. This change is due to the improved modeling of the central canal in CASMO-5M which allows representing this structure in its real orientation. A test calculation in which the canal was modeled parallel to the outer walls of the channel (i.e. the same as in CASMO-4E) produced almost the same fission rates as CASMO-4E for these rods.

Slightly higher fission rates in CASMO-5M than in CASMO-4E (average $\sim$0.7%) can be found for the UO_2 rods in the interior of the subbundles. The fission rates of peripheral rods are somewhat lower in CASMO-5M, the most marked changes being observed at the corners (in the 96-rod section, typically –0.7%) and in the rods next to them ($\sim$1% in the 92-rod section, but typically around 0.5% for the other two axial zones).

The total fission rates of the Gd-poisoned rods are typically about 1% lower in CASMO-5M than in CASMO-4E. This difference originates primarily from the fission rate of ^{238}U which is in average 3.5% lower for all the rods of the assembly in the CASMO-5M results than in those from CASMO-4E. Since ^{238}U accounts for approximately 15% of all the fissions in the Gd rods, but only for some 4% in the UO_2 rods, this reduces the relative fission rates of the former. This difference is opposite to that of the basic nuclear data. Comparison of the fission cross-sections for ^{238}U from ENDF/B-VII and ENDF/B-VI release 8 using JANIS [8] has shown that the former values are 1–2% higher over most of the relevant 2–11 MeV energy range. Other causes for the lower ^{238}U fission rate in CASMO-5M may be differences in the library group structures (66

a) 96-rod axial section

	10	9	8	7	6	5	4	3	2	1
J	0.978	0.993	0.999	0.997	0.996	0.989	0.986	0.998	1.021	0.970
I	1.012	0.976	1.007		1.001	0.990		1.005	0.986	1.002
H		1.006			1.000	0.996			1.005	0.994
G	1.010		1.005	0.975		0.996	0.979	1.014		0.996
F	0.990	1.008	1.008	1.010				0.991		1.003
E	0.990	1.002	0.997	0.985			0.999	0.993	1.007	
D			1.009	0.997	0.998	0.988	0.988	1.003		1.007
C	0.994	1.014		0.999	0.999	0.995	1.009		1.032	1.017
B	0.987	1.011	1.007		1.002	1.000		1.011	1.028	1.030
A	0.991	1.001	1.001	1.008	0.998	0.999	0.992	1.010	0.998	0.996

RMS = 1.2% Max. = 1.032 Min. = 0.970

b) 92-rod axial section

	10	9	8	7	6	5	4	3	2	1
J		1.011	0.987	0.988	0.994	1.000	0.996	1.013	1.012	
I	0.998	0.974	1.002		1.001	0.993		1.009	0.975	0.992
H	1.005	1.014		1.006		0.994	1.000		1.007	1.005
G	1.001		1.009	1.007	0.982	0.989		1.006		1.004
F	0.992	0.999	0.991	0.987			0.986		1.007	1.010
E	1.004	1.002					0.984		1.022	1.008
D	0.988		1.009	0.996	0.990	0.981	1.004	1.009		1.020
C	0.991	1.021		0.989	0.995	1.000	1.017		1.022	1.019
B	0.986	0.969	1.008		0.993	0.993		1.011	0.967	1.002
A		1.011	1.009	0.995	0.993	0.990	0.998	0.998	0.995	

RMS = 1.2% Max. = 1.022 Min. = 0.967

c) 84-rod axial section

	10	9	8	7	6	5	4	3	2	1
J		0.996	0.979	0.998	0.985	0.991	0.988	1.002	1.009	
I	0.992	0.954	1.006		0.999	0.997		1.021	0.964	0.984
H	1.001	1.031		1.008		0.996	1.008		1.029	0.994
G	1.005		1.008	0.968				1.008		1.003
F	0.984	0.999	0.993						1.001	0.992
E	0.992	1.001							1.014	1.003
D	0.989		1.006	0.984			0.982	1.002		1.003
C	0.995	1.013		0.998	0.997	0.997	1.014		1.027	1.010
B	0.986	0.969	1.015		0.989	1.001		0.996	0.965	1.005
A		1.018	0.993	1.014	0.994	0.996	1.008	0.990	1.014	

RMS = 1.5% Max. = 1.031 Min. = 0.954

Figure 3. C/E ratios for the CASMO-5M results (Gd-poisoned rods are shown with a shaded background)

groups above 0.821 MeV in CASMO-5M vs. 5 groups in CASMO-4E) or in the treatment of the fission spectrum.

The C/E ratios for the total fission rates calculated by CASMO-5M in each configuration can be found in Figure 3. The root-mean-square deviations for the 96 and 92-rod sections are almost the same as those found with CASMO-4E. For the 84-rod section, however, the deviation of the CASMO-5M results (1.5%) is higher than the corresponding value for CASMO-4E (1.2%). This appears to be a consequence of the fact that in this configuration the larger deviations of CASMO-5M for the Gd rods are not offset by the better agreement for the rods around the central canal (these rods are missing in the uppermost axial zone). All the rms deviations are clearly higher than the uncertainties of the measurements. The largest positive and negative deviations are typically in the order of 3% (except for some low C/E values for Gd rods in the 84-rod lattice).

The agreement of the total fission rates from CASMO-5M for the rods surrounding the central water canal with the experimental values is clearly better than for the CASMO-4E results. As discussed above, this is an effect of the improved geometrical modeling of the canal in CASMO-5M. An underprediction by approximately 1.5% can be seen for the 92-rod section, which should be compared to 2–3% for CASMO-4E. The fission rates of the UO_2 rods in the interior of the subbundles are slightly overestimated.

The fission rates of the Gd rods are underpredicted in average in all the configurations. Overestimates exceeding the experimental uncertainties are found for the two Gd rods near the south edge of the 96-rod section only. As in the case of CASMO-4E, the underprediction is more pronounced for a smaller number of rods in the lattice (and hence a softer neutron spectrum).

The CASMO-5M results for all the corner rods in the 96-rod lattice are lower than the measured values with a maximum difference of 3%. The fission rates of the rods next to the corners are generally well predicted, for a large majority of these rods within $\pm 1.5\%$.

As in the case of CASMO-4E, relatively high C/E values are somewhat concentrated near the southeast corner of the assembly, most conspicuously in the 96-rod section. The consistency between the two codes supports the suspicion that this trend may be related to some slight inaccuracy in the modeling of the test zone geometry.

5. CONCLUSIONS

Radial total fission rate distributions calculated using CASMO-4E and CASMO-5M have been compared to measurements performed in the three axial sections of an actual SVEA-96 Optima2 BWR fuel assembly in the PROTEUS zero-power experimental facility. Overall, the results of the two codes are very satisfactory, with rms deviations from the measured fission rates between 1.2% and 1.5% and maximum deviations of 3–4% in each case. Some slight systematic trends, with typical deviations in the order of 1–2%, have been observed for the fuel rods adjacent to the central water canal and to the outer corners of the assembly. The quality of the predictions by CASMO-4E and CASMO-5M is comparable. Compared to CASMO-4E, CASMO-5M shows an improvement for the fuel rods surrounding the central canal thanks to improved geometrical modeling, but also a more pronounced underestimate of the fission rates of Gd-poisoned fuel rods, particularly in the axial zones with a higher moderation ratio.

ACKNOWLEDGEMENTS

The LWR-PROTEUS program was conducted jointly by PSI and the Swiss nuclear utilities (swiss*nuclear*). The authors are indebted to J.-M. Cavedon and R. Brogli (PSI), J. Krouthén (AXPO Kernenergie AG), P. Hirt and G. Meier (Kernkraftwerk Gösgen), D. Furtado and U. Georg (Kernkraftwerk Mühleberg), H.-D. Berger (AREVA-ANP), and S. Helmersson (Westinghouse Electric Sweden) for their strong support of the experiments. Special thanks are due to M. Murphy, M. Plaschy and U. Bergmann for the precise experimental work and to R. Seiler, P. Bourquin, M. Fassbind and M. Zimmermann for reliable operation and maintenance of the PROTEUS reactor.

REFERENCES

[1] G. Perret, M. Plaschy, M.F. Murphy, F. Jatuff and R. Chawla, "Characterisation of Radial Reaction Rate Distributions Across the 92-Pin Section of a SVEA-96 Optima2 Assembly," *Ann. Nucl. Energy*, **35**, pp. 478–484 (2008).

[2] M.F. Murphy, F. Jatuff, G. Perret, M. Plaschy, U. Bergmann and R. Chawla, "Comparison of 3D Reaction Rate Distributions Measured in an Optima2 BWR Assembly with MCNPX Predictions," *Ann. Nucl. Energy*, **35**, pp. 2042–2050 (2008).

[3] G. Perret, M.F. Murphy, F. Jatuff and R. Chawla, "Fission Rate Distribution at the 84-pin Radial Section of a SVEA-96 Optima2 BWR Assembly," *Proceedings PHYSOR 2008*, Interlaken, Switzerland, September 14–19, 2008, on CDROM (2008).

[4] J. Rhodes, K. Smith and M. Edenius, *CASMO-4E, Extended Capability CASMO-4: User's Manual*, SSP-01/401 Rev 2, Studsvik Scandpower, Inc. (2004).

[5] J. Rhodes, K. Smith and D. Lee, *CASMO-5/CASMO-5M, a Fuel Assembly Burnup Program: User's Manual*, SSP-07/431 Rev 0, Studsvik Scandpower, Inc. (2007).

[6] D. B. Pelowitz, *MCNPX User's Manual Version 2.5.0*, LA-CP-05-0369 (2005).

[7] M. Murphy, A. Lüthi, R. Seiler, P. Grimm, O. Joneja, A. Meister, R. van Geemert, F. Jatuff, R. Brogli, R. Jacot-Guillarmod, T. Williams, S. Helmersson, R. Chawla, "Neutronics Investigations for the Lower Part of a Westinghouse SVEA-96+ Assembly," *Nucl. Sci. Eng.*, **141**, pp. 32–45 (2002).

[8] "Janis — A New Java-based Nuclear Data Display Program," OECD Nuclear Energy Agency (2001).